Robotics and Computer-Integrated Manufacturing 29 (2013) 417–423

Contents lists available at SciVerse ScienceDirect

Robotics and Computer-Integrated Manufacturing

journal homepage: www.elsevier.com/locate/rcim

# Modeling of bead section profile and overlapping beads with experimental validation for robotic GMAW-based rapid manufacturing

Jun Xiong, Guangjun Zhang*, Hongming Gao, Lin Wu

*State Key Laboratory of Advanced Welding and Joining, Harbin Institute of Technology, West straight street 92, Harbin 150001, PR China*

ARTICLE INFO

*Article history:*
Received 27 December 2011
Received in revised form
4 August 2012
Accepted 11 September 2012
Available online 3 October 2012

*Keywords:*
Rapid prototyping
Gas metal arc welding
Bead cross-section
Overlapping model

ABSTRACT

Robotic gas metal arc welding enables the capacity of fabricating fully dense components with low cost in rapid manufacturing. During the layer additive manufacturing, the cross-sectional profile of a single weld bead as well as overlapping parameters is critical for improving the surface quality, dimensional accuracy and mechanical performance. This paper highlights an experimental study carried out to determine the optimal model of the bead cross-section profile fitted with circular arc, parabola, and cosine function, by comparing the actual area of the bead section with the predicted areas of the three models. A necessary condition for the overlapping of adjacent beads is proposed. The results show that different models for the single bead section profile result in different center distances and surface qualities of adjacent beads. The optimal model for the bead section profile has an important bearing on the ratio of wire feed rate to welding speed.



## 1. Introduction

Layer additive manufacturing is an important topic for fabricating 3D functional metal objects directly from CAD model of parts. Recently, rapid prototyping/manufacturing (RP) using laser as the heat source has gained wide popularity due to its low heat input, high precision and less susceptible to distortion. Abe et al. [1] proposed a selective laser melting approach that metallic powders were continuously melted and solidified in a microscopic zone. And a dual scanning system was developed. An RP technology with laser additive manufacture of wire based alloy Ti–6Al–4V, proposed by Miranda et al. [2], was used for the production of cylindrical components by using a high power fiber laser. For fabrication of thin-walled parts of nickel alloy with uniform height by using closed-loop control, Li et al. [3] developed a direct laser fabrication system consisting of a $CO_2$ laser, a 3-axis CNC table, a coaxial power nozzle and a power recycler. However, disadvantages of using laser as the energy source lie in complex laser beam delivery mechanism and high production costs.

For acquiring metallic objects with excellent properties, high density and good bonding strength, the weld-based RP process using gas metal arc welding (GMAW) has been demonstrated to be powerful [4]. It has advantages of high efficiency, low cost, and simple equipment. In this field, Spencer et al. [5] fabricated several parts with a GMAW-based RP system, and temperature control techniques were employed to improve the surface finish. A multivariable adaptive modeling and control process of bead geometry in GMAW material deposition with application in solid freeform fabrication (SFF) was developed by Doumanidis and Kwak [6]. Zhang et al. [7] established an RP system by using GMAW as the layered deposition technique, and several complicated parts were fabricated. Song and Park [8] as well as Karunakaran et al. [9] studied 3D welding and milling techniques for improving surface quality and accuracy of SFF parts.

The crucial idea of RP is an additive manufacturing process that slices complex 3D geometry into simple 2.5D features along the vertical direction [10]. It is composed of establishment of 3D models of products, calculation of expected thickness and design of the welding path and parameters in each layer, communication with the robot, and stacking up of deposited beads layer by layer. In addition to weld bead width and height, the profile and area of the cross-section of a single weld bead as well as overlapping parameters of adjacent beads have great influence on the surface quality, dimensional accuracy and mechanical performance.

Many researches [11–14] have been focused on developing models between welding parameters and bead width, height, and penetration in joining applications using regression analysis and neural networks, without further research of the weld bead profile. Aiyiti et al. [15] proposed an RP system based on the micro-plasma arc welding, and qualitatively assumed the bead profile as a circular arc. Spencer et al. [5] and Chan et al. [16] regarded the bead profile as a parabola without the verification test. The points of bead boundary were fitted with Gaussian,

* Corresponding author. Tel./fax: +86 451 86415537.
*E-mail address:* zhanggj@hit.edu.cn (G. Zhang).

0736-5845/$ - see front matter © 2012 Elsevier Ltd. All rights reserved.
http://dx.doi.org/10.1016/j.rcim.2012.09.011

logistic, parabola and sine function by Cao et al. [17], the sine function has highest accuracy to fit the measured data, but only one combination of process parameters was performed. Suryakumar et al. [18] assumed a symmetric parabola profile of the weld bead and fitted the boundary points by the parabola function with experimental validation. Unfortunately, previous studies on bead cross-section profile are inadequate due to lack of verification tests used for quantitative assessments.

The aim of this study is to model the bead profile by means of three frequently-used curves, namely circular arc, parabola, and cosine function. The areas of the bead cross-section, predicted by the three models, are compared with that of the measured weld beads under different combinations of welding parameters, respectively. The optimal model of the single bead profile is used to determine the overlapping distance of adjacent beads in the robotic GMAW-based RP process.

## 2. Overlapping model and three single bead models

### 2.1. Principle of the overlapping model

Unlike the single weld bead in joining applications, each layer in the GMAW-based deposition process consists of continuous overlapping beads. A simple sketch of the overlapping model is shown in Fig. 1. The area of valley and overlapping area in adjacent beads are depicted. The center distance of adjacent beads is defined as $d$.

With a view to simplifying the overlapping model, three assumptions are proposed:

(1) The cross-section profile of a single weld bead is symmetrical.
(2) Every weld bead with the same welding parameter has uniform cross-section profile.
(3) The section profile of a single weld bead remains unchanged during the overlapping of adjacent beads.

The center distance of adjacent beads plays an important role in the determination of surface quality and smoothness. As shown in Fig. 2, different center distances cause different layer thickness and surface smoothness. When the center distance is greater than the single bead width $w$, there is no overlapping material between adjacent beads, as seen in Fig. 2(a). With a decrease of the center distance, the smoothness in the deposited layer becomes better and better, as shown in Fig. 2(b). This is because the overlapping area fills the area of the valley automatically. As the center distance decreases to a certain value, the overlapping area is equal to the area of the valley; the overlapping surface will become an optimal plane, as shown in Fig. 2(c). With a further decrease of the center distance, excessive overlapping area leads to an increased thickness of the deposited layer and worse surface smoothness, as shown in Fig. 2(d), which is not expected in layer additive manufacturing.

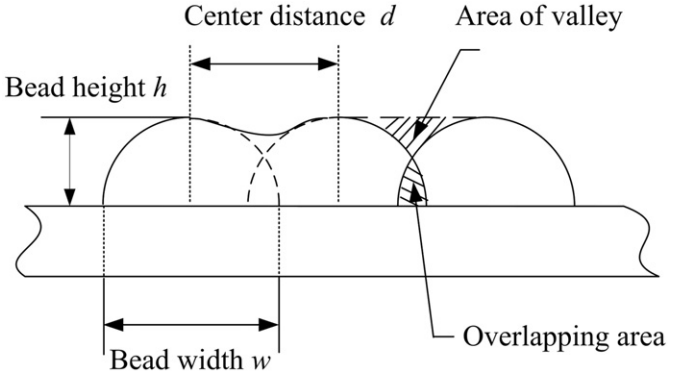


**Fig. 1.** Sketch of overlapping beads.

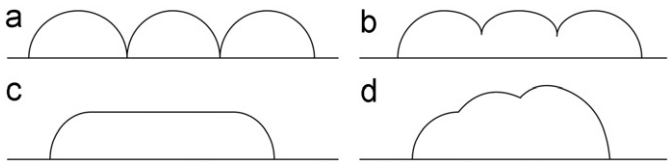


**Fig. 2.** Patterns of different center distance $d$. (a) $d$ more than $w$, (b) $d$ less than $w$, overlapping area less than area of valley (c) $d$ less than $w$, overlapping area equal to area of valley, (d) $d$ less than $w$, overlapping area more than area of valley.

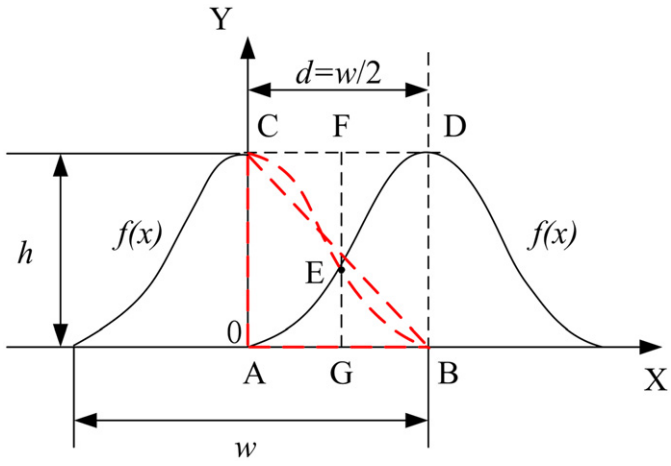


**Fig. 3.** Overlapping pattern as $d=w/2$.

### 2.2. A necessary condition for overlapping beads

The variation range of the center distance is from $w/2$ to $w$ in the layered deposition process. This is due to the fact that when the center distance is larger than $w$, there is no overlapping area between adjacent beads. As the center distance is less than $w/2$, the welding path is located on the adjacent bead. This will re-melt the adjacent bead excessively, and the bonding strength of the current weld bead with the substrate or previous layers may be inadequate. Fig. 3 shows an overlapping model when center distance is equal to $w/2$. The function curve of the actual bead cross-section is expressed as $f(x)$. Point E is the point of interaction between two adjacent beads.

One of the extreme cases is that when $d$ is equal to $w/2$, the area of the valley should be less than the overlapping area. Then, with the increase of $d$, the area of the valley increases and the overlapping area decreases. At an optimal center distance, the area of valley will be equal to the overlapping area. Consequently, a necessary condition for the overlapping beads is that when $d$ is equal to $w/2$, the area of the valley is less than the overlapping area, namely;

$$\begin{aligned}
&\text{Area (CED)} \le \text{Area (AEB)}\\
&\Rightarrow 2\times\text{Area (CE}F\text{)} \le \ 2\times\text{Area (GEB)}\\
&\Rightarrow 2\times\text{Area (CE}F\text{)} \le 2\times\text{Area (GEB)}\\
&\Rightarrow \text{Area (CE}F\text{)} \le \text{Area (GEB)}\\
&\Rightarrow \int_0^{w/4}(h-f(x))dx \le \int_{w/4}^{w/2} f(x)dx\\
&\Rightarrow \int_0^{w/2} f(x)dx \ge wh/4 \qquad (1)
\end{aligned}$$

Thus, half of the area of the weld bead cross-section should be larger than the area of the triangle ABC, as shown in Fig. 3. In order to meet this condition, the weld bead profile $f(x)$ had better be a convex function in the closed interval [0, $w/2$].

### 2.3. Three models for the single bead profile

As discussed in Section 1, the profile of the single bead is frequently fitted by three curve functions, namely parabola, circular arc, and cosine function. So the three models are to be developed. Fig. 4 depicts the single bead profile above the substrate or previous layers.

(1) Parabola model

The algebraic form of a parabola can be expressed as $y=ax^2+c$, and the curve passes through point $B$ ($w/2$, 0) and $C$ (0, $h$), so the formulation can be written as follows:

$$y=-\frac{4h}{w^2}x^2+h \tag{2}$$

The area of the parabola profile is calculated as

$$A_p=\int_{-w/2}^{w/2}\left(-\frac{4h}{w^2}x^2+h\right)dx=\frac{2wh}{3} \tag{3}$$

(2) Cosine model

The algebraic form of a cosine can be written as $y=a\cos bx$, and the curve passes through point $B$ ($w/2$, 0) and $C$ (0, $h$), so the formulation can be expressed as

$$y=h\cos(\pi x/w) \tag{4}$$

The area of the cosine profile is calculated as

$$A_c=\int_{-w/2}^{w/2}h\cos(\pi x/w)dx=\frac{2wh}{\pi} \tag{5}$$

(3) Arc model

The algebraic form of a circular arc can be expressed as $(x-a)^2+(y-b)^2=R^2$, $R$ is the radius of the arc, and the curve passes through point $B$ ($w/2$, 0) and $C$ (0, $h$), so the formulation can be written as follows:

$$R=\frac{(h^2+w^2/4)}{2h} \tag{6}$$

$$y=\sqrt{R^2-x^2}+h-R \tag{7}$$

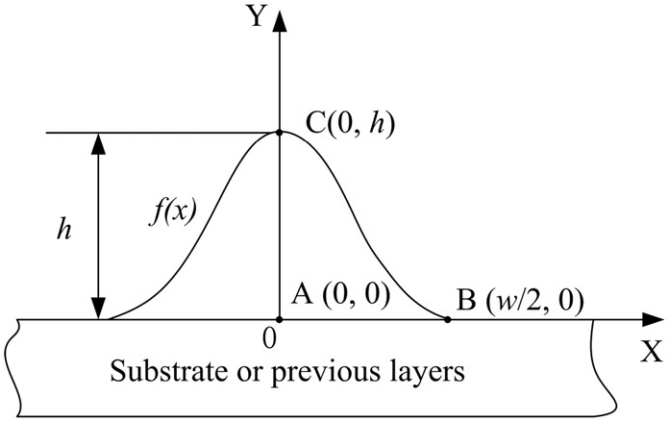


**Fig. 4.** Cross-section profile of a single weld bead.

The area of the arc profile is calculated as

$$A_a=\int_{-w/2}^{w/2}(\sqrt{R^2-x^2}+h-R)\,dx$$

$$\Rightarrow A_a=R^2\arcsin\frac{w}{2R}+\frac{w\sqrt{R^2-w^2/4}}{2}+w(h-R) \tag{8}$$

## 3. Experimental verification of single bead models

As shown in Fig. 5, curve $C_0$ is the actual bead cross-section profile; curves $C_1$ and $C_2$ are two hypothetic bead section models with less and more area compared with that of $C_0$, respectively. $C'_0$, $C'_1$ and $C'_2$ are their corresponding adjacent beads. Based on the theory that the overlapping area is equal to the area of the valley, the desired center distances, namely $d_0$, $d_1$, and $d_2$, are determined. It can be seen that the curve model with less area results in less center distance, and *vice versa*. Consequently, the area of the bead profile plays an important role in determining the desired center distance. In order to select a most accurate curve model, the area of the bead cross-section predicted with models should be compared with the measured area.

The area of the weld bead cross-section, namely metal deposition rate per unit length, is expressed as

$$A_m=\frac{\pi V_w D_w^2}{(4V_s)} \tag{9}$$

where $V_w$ is the wire feed rate, $D_w$ is the diameter of the wire electrode, and $V_s$ is the welding speed.

The robotic GMAW-based RP system is presented in Fig. 6. A motoman UP20 robot manipulator was applied to control the welding process. A Fronius TPS5000 was employed as the welding power supply. A unified adjustment of welding parameters was used and the welding current increases along with wire feed rate. The wire electrode was copper coated steel wire of 1.2 mm diameter with composition of C (0.11% maximum), Si (0.65–0.95), Mn (1.8%-2.1%), Ni (0.3 maximum) and Cr (0.2 maximum). Ar (95%) and $CO_2$ (5%) gas mixture was the shielding gas with a flow rate of 18 L/min. Experiments with different combinations of welding speed and wire feed rate were performed on an MS substrate of 210 mm × 120 mm × 9.5 mm. The wire feed rate ranges from 2.8 to 6 m/min and the welding speed is varied from 15 to 45 cm/min. The nozzle-to-plate distance was fixed properly, avoiding the presence of spatters as possible.

As shown in Fig. 6, a laser vision sensor projecting a laser line on the weld bead profile was used to measure the bead width $w$ and height $h$ of the single bead. The vision sensor consists of a laser diode with power of 30 mW emitting at 650 nm and a CCD

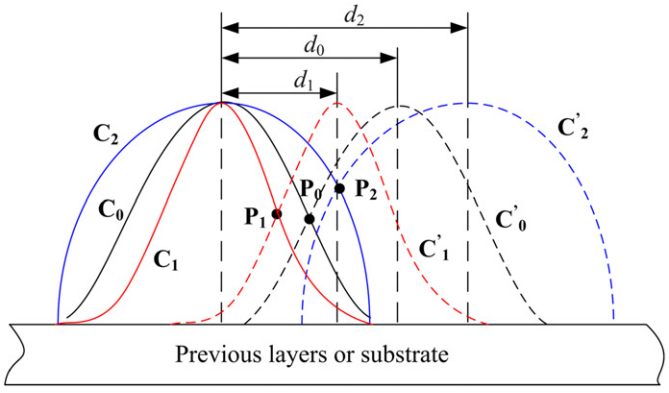


**Fig. 5.** Geometry of overlapping with different models of single bead.

camera. A narrow-band filter with the center wavelength corresponding to the laser diode and a neutral filter were placed in front of the camera to reduce noises. The camera is able to acquire 8 bit gray scale image. The laser vision sensor was calibrated accurately by applying a precisely machined steel bar with step gradations. Every bead width and height was measured for three times at different locations except for arc striking and extinguishing points.

Table 1 shows the measured bead geometry produced by different combinations of process parameters, and the comparisons of actual areas with predicted cross-sectional areas based on the three models. The accuracy of areas predicted by the three models was evaluated by the mean value of the error rate (ER) and the standard deviation of the ER. The ER is defined by Eq. (10).

$$ER_{(n)} = \frac{|A_{predicted(n)} - A_{actual(n)}|}{A_{actual(n)}} \times 100\% \quad (10)$$

where $A_{predicted(n)}$ is the predicted area based on the three models, $A_{actual(n)}$ is the actual area of the weld bead cross-section, and $n$ is the experiment index.

The relative error (RE) between the actual area and the predicted area is calculated as

$$RE_{(n)} = \frac{A_{predicted(n)} - A_{actual(n)}}{A_{actual(n)}} \times 100\% \quad (11)$$

The relative errors of the three models, compared with the actual area of the single bead cross-section, are shown in Fig. 7 by drawing scatter points. It is clearly seen that the maximum errors of the arc, cosine, and parabola model are 20.7%, 16.54% and 12.61%, respectively. The parabola model gives the mean value and standard deviation of the ER as 5.952% and 2.997%, respectively; whereas the cosine model results in corresponding values as 8.036% and 4.256%, respectively and the arc model are 7.502% and 6.078%, respectively. The error curve of the parabola model is

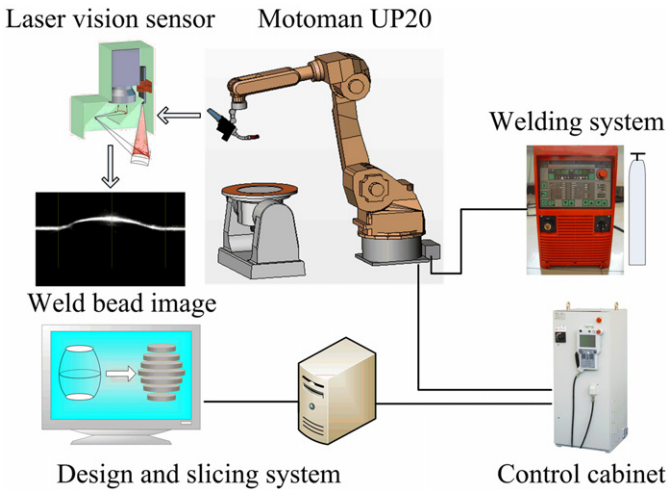


**Fig. 6.** Schematic diagram of the experimental set-up.

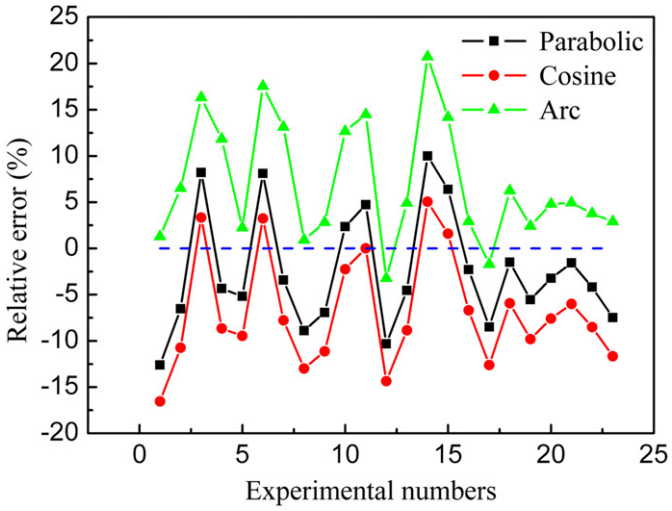


**Fig. 7.** Comparison of relative error for actual and predicted area of weld bead cross-section.

**Table 1**
Comparison of actual and predicted areas of the bead cross-section.

| S. No | Process parameters | | Measured geometry | | Real area | Predicted area | | |
|---|---|---|---|---|---|---|---|---|
| | $V_w$ (m/min) | $V_s$ (cm/min) | $w$ (mm) | $h$ (mm) | $A_m$ (mm$^2$) | $A_p$ (mm$^2$) | $A_c$ (mm$^2$) | $A_a$ (mm$^2$) |
| 1 | 2.8 | 21 | 6.488 | 3.047 | 15.08 | 13.178 | 12.584 | 15.273 |
| 2 | 2.8 | 27 | 6.128 | 2.683 | 11.729 | 10.962 | 10.467 | 12.494 |
| 3 | 2.8 | 30 | 7.387 | 2.319 | 10.556 | 11.422 | 10.907 | 12.278 |
| 4 | 2.8 | 37.5 | 4.994 | 2.426 | 8.445 | 8.078 | 7.714 | 9.444 |
| 5 | 3.6 | 22.5 | 8.95 | 2.876 | 18.096 | 17.158 | 16.385 | 18.501 |
| 6 | 3.6 | 37.5 | 7.193 | 2.448 | 10.858 | 11.738 | 11.209 | 12.763 |
| 7 | 3.6 | 45 | 5.174 | 2.533 | 9.048 | 8.738 | 8.344 | 10.236 |
| 8 | 4 | 21 | 8.798 | 3.346 | 21.543 | 19.628 | 18.743 | 21.740 |
| 9 | 4 | 27 | 7.899 | 2.961 | 16.756 | 15.594 | 14.891 | 17.227 |
| 10 | 4 | 36 | 7.249 | 2.662 | 12.567 | 12.863 | 12.283 | 14.159 |
| 11 | 4 | 39 | 7.193 | 2.533 | 11.6 | 12.149 | 11.601 | 13.280 |
| 12 | 4.4 | 15 | 11.759 | 3.796 | 33.176 | 29.754 | 28.413 | 32.104 |
| 13 | 4.4 | 30 | 8.079 | 2.940 | 16.588 | 15.833 | 15.119 | 17.402 |
| 14 | 4.4 | 37.5 | 7.788 | 2.811 | 13.270 | 14.596 | 13.940 | 16.022 |
| 15 | 4.4 | 45 | 7.539 | 2.341 | 11.059 | 11.765 | 11.235 | 12.628 |
| 16 | 4.6 | 40 | 8.51 | 2.24 | 13.007 | 12.708 | 12.136 | 13.387 |
| 17 | 5.2 | 22.5 | 10.721 | 3.346 | 26.139 | 23.917 | 22.839 | 25.689 |
| 18 | 5.2 | 27 | 10.002 | 3.218 | 21.782 | 21.456 | 20.489 | 23.141 |
| 19 | 5.2 | 30 | 9.116 | 3.047 | 19.604 | 18.517 | 17.682 | 20.079 |
| 20 | 5.2 | 37.5 | 8.286 | 2.747 | 15.683 | 15.176 | 14.492 | 16.438 |
| 21 | 6 | 27 | 11.233 | 3.304 | 25.133 | 24.739 | 23.624 | 26.374 |
| 22 | 6 | 30 | 9.905 | 3.282 | 22.62 | 21.672 | 20.696 | 23.472 |
| 23 | 6 | 45 | 7.332 | 2.854 | 15.08 | 13.951 | 13.322 | 15.520 |

uniformly distributed on both sides of the dash line. Comprehensively, the area predicted by the parabola model is more accurate.

The influence of the ratio of wire feed rate to welding speed (RWFRWS) on the relative error is displayed in Fig. 8. As RWFRWS is less than 12.5, errors predicted by the arc model are conspicuously larger than that of the other two models. The mean value and standard deviation of the ER based on the parabola model are 5.64% and 2.635%, respectively; the corresponding values from the cosine model are 4.936% and 3.447%. The error analysis demonstrates that there is no distinct difference for the accuracy of both models. For a stable accuracy of the bead section profile, the parabola model with less standard deviation of the ER is preferred. When RWFRWS varies from 12.5 to 30, the cross-sectional areas predicted by the cosine model are less accurate than that of the other two models. The parabola model gives the mean value and standard deviation of the ER as 6.192% and 3.334%, respectively; whereas the arc model results in corresponding values as 3.246% and 1.604%, respectively. Therefore, the arc model is superior to the parabola model.

Experimental results show that when RWFRWS is large, the surface appearance of the weld bead is similar to an arc, as shown in Fig. 9(a). As RWFRWS is relatively small, the surface appearance of the weld bead is close to a triangle, as seen in Fig. 9(b). This is due to the fact that the decrease of RWFRWS results in decreased metal deposition rate per unit length and the heat input. The heat dissipation of the increased pool size is fast, and droplets transferred to the top surface of the weld pool are easy to be solidified. On the contrary, as RWFRWS is large, the heat dissipation of the increased pool size is slow, which make droplets transferred to the top surface of the weld pool flow easily. Before droplets flowing to the substrate, they may be solidified. Thus, the bead cross-section profile is shown to be an arc.

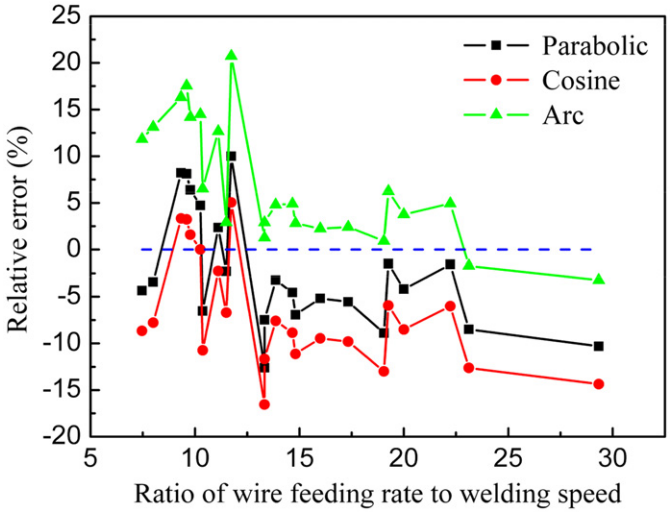


**Fig. 8.** Effect of ratio of wire feed rate to welding speed on relative error.

## 4. Center distance of multi-bead deposition

In the robotic GMAW-based RP process, each layer is deposited by many overlapping beads. The center distance of adjacent beads has a great effect on the surface smoothness and dimension. The sketch of the overlapping model for adjacent beads is shown in Fig. 10. Point E with the coordinate $(x_E, y_E)$ is the point of interaction between two overlapping beads. Based on the three assumptions proposed in Section 2.1, as the overlapping area is equal to the area of the valley, the optimal center distance can be calculated.

As the ratio of the wire feed rate to the welding speed is less than 12.5, the cross-section profile should be fitted with a parabola curve.

$$f(x) = -\frac{4h}{w^2}x^2 + h$$

$$\text{Area(CED)} = \text{Area(AEB)}$$

$$\Rightarrow 2 \times \text{Area(CE}F\text{)} = 2 \times \text{Area(GEB)}$$

$$\Rightarrow \int_0^{x_E}\left[h-\left(h-\frac{4h}{w^2}x^2\right)\right]dx = \int_{x_E}^{w/2}\left(h-\frac{4h}{w^2}x^2\right)dx$$

$$\Rightarrow x_E = w/3 \tag{12}$$

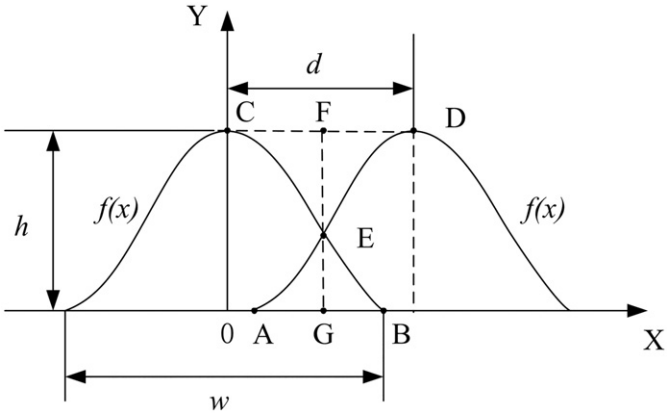


**Fig. 10.** Sketch of the overlapping model for adjacent beads.

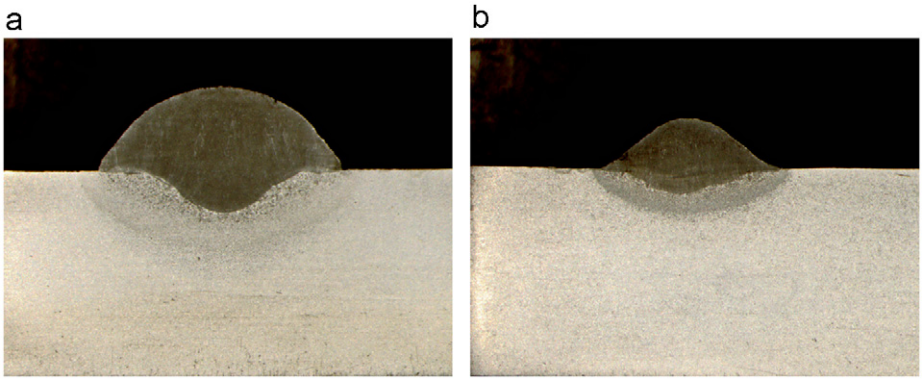


**Fig. 9.** Macrosection of different RWFRWS. (a) RWFRWS=29.3 (b) RWFRWS=9.7.

So the optimal center distance of overlapping beads can be obtained:

$$d = 2w/3 \tag{13}$$

When the ratio of the wire feed rate to the welding speed is more than 12.5, the cross-section profile should be fitted with an arc curve.

$$f(x) = \sqrt{R^2 - x^2} + h - R$$

$$R = \frac{(h^2 + w^2/4)}{2h}$$

$$\text{Area(CED)} = \text{Area(AEB)}$$

$$\Rightarrow 2 \times \text{Area(CE}F\text{)} = 2 \times \text{Area(GEB)}$$

$$\Rightarrow \text{Area(CE}F\text{)} = \text{Area(GEB)}$$

$$\Rightarrow \int_0^{x_E} \left[h - (\sqrt{R^2 - x^2} + h - R)\right] dx = \int_{x_E}^{w/2} (\sqrt{R^2 - x^2} + h - R) dx$$

$$\Rightarrow x_E = \frac{1}{4h}\left(2R^2 \arcsin\frac{w}{2R} + wh - wR\right) \tag{14}$$

So the optimal center distance of overlapping beads can be obtained:

$$d = \frac{1}{2h}\left(2R^2 \arcsin\frac{w}{2R} + wh - wR\right) \tag{15}$$

Table 2 shows the center distances of adjacent beads calculated with parabola and arc functions under two different process parameters. The RWFRWS of experiment one is 22.222. The optimal center distance predicted by both models presents different values. Fig. 11 displays the overlapped surface of three deposited beads using both models. There is some small concavity on the top surface shown in Fig. 11(a) due to the effect of surface tension. As seen in Fig. 11(b), the thickness of the latter bead is greater than the former bead, which increases the layer thickness and decreases the efficiency of the layered deposition process.

The RWFRWS of experiment two is 10.256. The center distances calculated by means of both models are different. Fig. 12 shows the overlapped surface of three deposited beads using different models. It can be observed that the surface smoothness in Fig. 12(a) is superior to that in Fig. 12(b). There is an obvious concave at the connection point in Fig. 12(b), which may affect the quality of the subsequent layers.

## 5. Conclusions

The models of the single bead cross-section profile have been developed by means of parabola, arc, and cosine functions,

**Table 2**
Center distance calculated with parabola and arc models.

| S. No. | Process parameters | | RWFRWS | Bead geometry | | Center distance (mm) | |
|---|---|---|---|---|---|---|---|
| | $V_w$ (m/min) | $V_s$ (cm/min) | | $w$ (mm) | $h$ (mm) | Parabola function | Arc function |
| 1 | 4 | 18 | 22.222 | 9.2 | 3.6 | 6.133 | 6.829 |
| 2 | 4 | 39 | 10.256 | 7.193 | 2.533 | 4.760 | 5.242 |

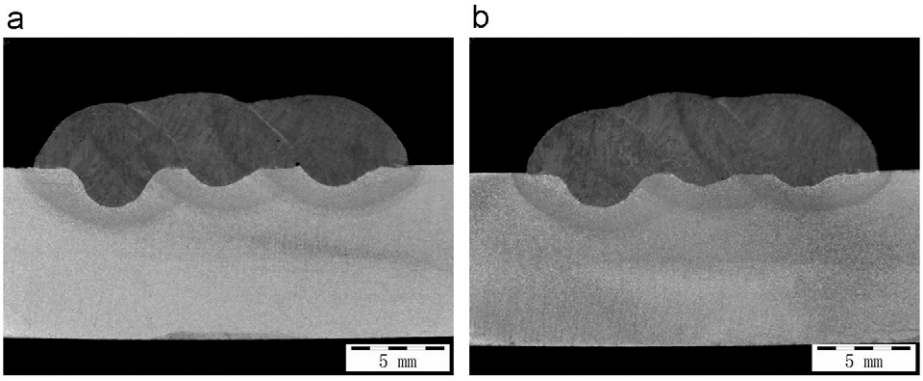


**Fig. 11.** Overlapping results with different models when RWFRWS=22.222. (a) Arc model. (b) Parabola model.

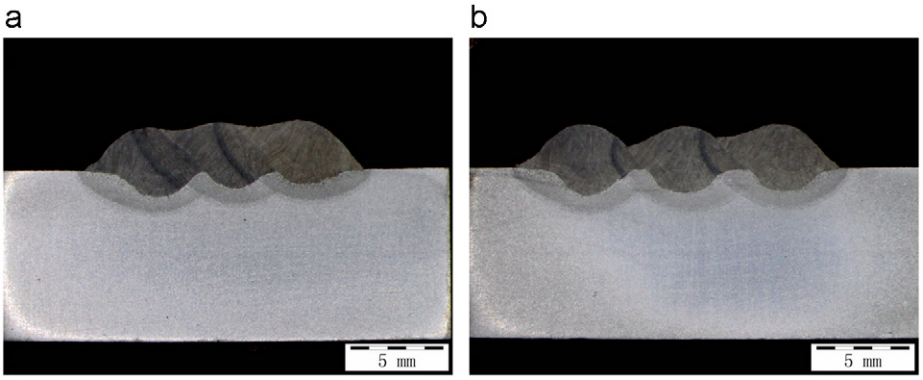


**Fig. 12.** Overlapping results with different models when RWFRWS=10.256. (a) Parabola model. (b) Arc model.

respectively. A necessary condition for the overlapping of adjacent beads is that the bead section profile had better be a concave function. The experimental investigation with different combinations of process parameters has been used to determine the optimal model by comparing the actual area of the bead section with that predicted by the three models. Significant results indicate that the ratio of wire feed rate to welding speed greatly influence the shape of the bead profile. As the ratio of the wire feed rate to the welding speed is more than 12.5, the arc model for the single bead section profile has higher accuracy than the other two functions. When it is less than 12.5, the parabola model is more reasonable. Based on the determined optimum model for the single bead section, the center distance of adjacent beads is calculated and smooth surface of the deposited layer is obtained with no defects.

## Acknowledgments

This work was supported by National Natural Science Foundation of China, No. 51175119.

## References

[1] Abe F, Osakada K, Shiomi M, Uematsu K, Matsumoto M. The manufacturing of hard tools from metallic powders by selective laser melting. Journal of Materials Processing Technology 2001;111:210–3.
[2] Miranda RM, Lopes G, Quintino L, Rodrigues JP, Williams S. Rapid prototyping with high power fiber lasers. Materials and Design 2008;29:2072–5.
[3] Li P, Ji SQ, Zeng XY, Hu QW, Xiong WH. Direct laser fabrication of thin-walled metal parts under open-loop control,. International Journal of Machine Tools and Manufacture 2007;47:996–1002.
[4] Mughal MP, Fawad H, Mufti RA. Three-dimensional finite-element modelling of deformation in weld-based rapid prototyping. Proceedings of the Institute of Mechanical Engineering: Mechanical Engineering Science 2006;220(6): 875–85.
[5] Spencer JD, Dickens PM, Wykes CM. Rapid prototyping of metal parts by three-dimensional welding. Proceedings of the Institute of Mechanical Engineering: The Journal of Engineering Manufacture 1998;212:175–82.
[6] Doumanidis C, Kwak YM. Multivariable adaptive control of the bead profile geometry in gas metal arc welding with thermal scanning. International Journal of Pressure Vessels and Piping 2002;79:251–62.
[7] Zhang YM, Chen Y, Li P, Male AT. Weld deposition-based rapid prototyping a preliminary study. Journal of Materials Processing Technology 2003;135(2–3): 347–57.
[8] Song YA, Park S. Experimental investigations into rapid prototyping of composites by novel hybrid deposition process. Journal of Materials Processing Technology 2006;171:35–40.
[9] Karunakaran KP, Suryakumar S, Pushpa V, Akula S. Low cost integration of additive and subtractive processes for hybrid layered manufacturing. Robotics and Computer-Integrated Manufacturing 2010;26:490–9.
[10] Weiss LE, Prinz FB, Adams DA, Siewiorek DP. Thermal spray shape deposition. Journal of Thermal Spray Technology 1992;1(13):231–7.
[11] Kim IS, Son JS, Lee SH, Yarlagadda PKDV. Optimal design of neural networks for control in robotic arc welding. Robotics and Computer-Integrated Manufacturing 2004;20:57–63.
[12] Kannan T, Murugan N. Effect of flux cored arc welding process parameters on duplex stainless steel clad quality. Journal of Materials Processing Technology 2006;176:230–9.
[13] Kim IS, Son JS, Yarlagadda PKDV. A study on the quality improvement of robotic GMA welding process. Robotics and Computer-Integrated Manufacturing 2003;19:567–72.
[14] Palani PK, Murugan N. Optimization of weld bead geometry for stainless steel claddings deposited by FCAW. Journal of Materials Processing Technology 2007;190:291–9.
[15] Aiyiti W, Zhao W, Lu B, Tang Y. Investigation of the overlapping parameters of MPAW-based rapid prototyping. Rapid Prototyping Journal 2006;12(3): 165–72.
[16] Chan B, Pacey J, Bibby M. Modelling gas metal arc weld geometry using artificial neural network technology. Canadian Metallurgical Quarterly 1999;38(1):43–51.
[17] Cao Y, Zhu S, Liang XB, Wang WL. Overlapping model of beads and curve fitting of bead section for rapid manufacturing by robotic MAG welding process. Robotics and Computer-Integrated Manufacturing 2011;27:641–5.
[18] Suryakumar S, Karunakaran KP, Bernard A, Chandrasekhar U, Raghavender N, Sharma D. Weld bead modeling and process optimization in hybrid layered manufacturing. Computer Aided Design 2011;43:331–44.